34th Annual International Conference of the IEEE EMBS
San Diego, California USA, 28 August - 1 September, 2012

Implantable Multilayer Microstrip Antenna for Retinal Prosthesis: Antenna Testing

Hans Permana, *Student Member, IEEE*, Qiang Fang, *Member, IEEE*, and Wayne S. T. Rowe, *Member, IEEE*

Abstract— **Retinal prosthesis has come to a more mature stage and become a very strategic answer to Retinitis Pigmentosa (RP) and Age-related Macular Degeneration (AMD) diseases. In a retinal prosthesis system, wireless link holds a great importance for the continuity of the system. In this paper, an implantable multilayer microstrip antenna was proposed for the retinal prosthesis system. Simulations were performed in High Frequency Structure Simulator (HFSS) with the surrounding material of air and Vitreous Humor fluid. The fabricated antenna was measured for characteristic validation in free space. The results showed that the real antenna possessed similar return loss and radiation pattern, while there was discrepancy with the gain values.**

I. Introduction

Age-related Macular Degeneration (AMD) is an ocular disease that affects one's vision and progressively leads to blindness. It is one of the leading causes of irreversible blindness in the world with the total cost of US$ 343 billion worldwide [1]. Retinitis Pigmentosa (RP) is another eye disease that is primarily caused by a degeneration of the photoreceptor cells. Patients of this disease lose their sight progressively and eventually experience a complete blindness. The prevalence of RP is 1 in 4000 that translates to 1 million people worldwide [2]. Retinal prosthesis is aimed to assist affected individuals by generating artificial visual perception to do some basic daily activities.

There are two types of retinal prosthesis systems based on the electrodes placement, epiretinal and subretinal. However, the term retinal prosthesis in this paper will refer only to the epiretinal implant. Extensive studies on retinal prosthesis that involved animal or human testing have been conducted by multiple groups of researchers around the world with diverse point of emphasis among them. This group [3-4] set the focus on the development of advanced surgical procedure as well as the thermal exposure analysis on the surrounding area. Clinical trials have been conducted on blind people as the test subjects to test the feasibility of the system [5]. Another group have been conducting comprehensive studies on the electrode material of the implants [6]. This group had achieved an electrode array size of 16x16 for retinal stimulation, which had been tested on rabbit's eye [7-8]. There is also one group that have a unique approach by modelling retinal cell in regards to the electrical stimulation. The response of the ganglion cells, as a result of various stimulations, was investigated by software simulations [9]. Rabbit retina was implemented in *in vitro* experiment for result validation [10].

For all epiretinal implants, the system comprises an external camera and intraocular electrodes. As a result, a wireless communication between those two parts is required. The presence of antenna in the system is essential, to provide a reliable data transfer among the two components. In [11], preliminary analysis has been conducted to define the constraints of the implantable antenna. Various simulations have also been performed to find the best possible results using the given conditions. It was concluded that multilayer mirostrip antenna is the most suitable antenna in this circumstances, due to its size and biocompatibility.

In this paper, an improved version of multilayer microstrip antenna was designed, simulated, and tested in free space. The detail of the experiment will be presented in the following organization: the first section will cover the introduction; the second part will cover the simulation details. The measurement procedures as well as the measurement results will be on the following section. Section four will cover the analysis of the obtained data. Finally, Future Works and Conclusions completed the paper.

II. Antenna Design and Simulation

A. Antenna Design

The antenna was designed with the aid of HFSS software. Structurally, the antenna consists of four microstrip layers with each of them separated by thin layer of RO3210 substrates. The first three layers are connected in multiple locations by two pins (shorting pin and feed pin). The pattern of each layer can be seen on Fig. 1. A layer of polydimethylsiloxane (PDMS) is then added to provide biocompatible characteristic to the antenna. In the simulation, the antenna was implanted inside a sphere of Vitreous Humor fluid (ε_r = 69, σ=1.5296 S/m at 402 MHz) [12] to replicate the real-life condition inside the eyeball.

B. Simulation Parameters

As previously stated, the simulation was performed with the aid of HFSS software package with the solution frequency of 402 MHz. The input power to the antenna was by default set to 1W. An outer spherical boundary was added

H. Permana is with the School of Electrical and Computer Engineering, RMIT University, Melbourne, VIC, 3000, Australia. (phone: +61 3 99253025; fax: +61 3 99252007; e-mail: hans.permana@rmit.edu.au).

Q. Fang is with the School of Electrical and Computer Engineering, RMIT University, Melbourne, VIC, 3000, Australia. (e-mail: john.fang@rmit.edu.au).

W. S. T. Rowe is with the School of Electrical and Computer Engineering, RMIT University, Melbourne, VIC, 3000, Australia, (e-mail: wayne.rowe@rmit.edu.au).

to resemble infinite radiation boundary for the purpose of obtaining far field pattern of the antenna.

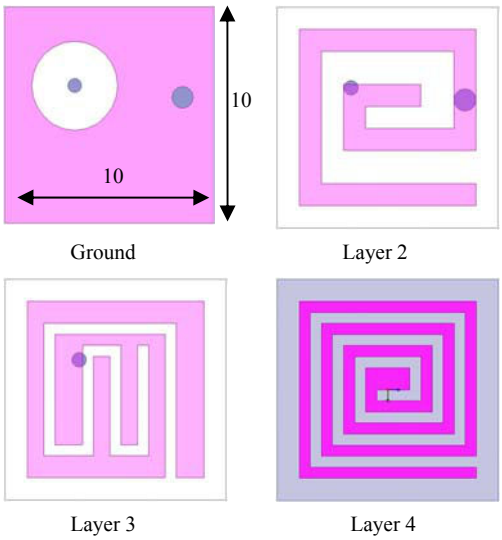

Figure. 1. The top view of each antenna layer

The antenna was simulated in three conditions in order to simplify the verification process of the fabricated one:

- Simulation in free space without PDMS encapsulation.
- Simulation in free space with PDMS layer.
- Simulation in Vitreous Humor with PDMS layer.

Other parameters remained unchanged during the simulations.

There are three antenna properties that were observed during the simulation and the measurement process: return loss, gain, and radiation pattern.

C. Simulation Results

The return loss of the antenna can be seen at Fig. 2. The antenna was specifically designed to operate optimally inside Vitreous Humor fluid. Therefore, resonance frequency of 402.8 MHz was obtained in this set up (blue line). In the free space, the antenna was resonant at higher frequency of 408.8 MHz (with PDMS enclosure) and 410 MHz (without the enclosure), marked by the red and black line in the chart, respectively.

The radiation pattern of the antenna in all simulation set ups was omnidirectional with the maximum gain achieved at the side of the antenna. It was influenced by the size of the antenna which was much smaller than the wavelength. The maximum gain for each set up can be observed at the Table 1.

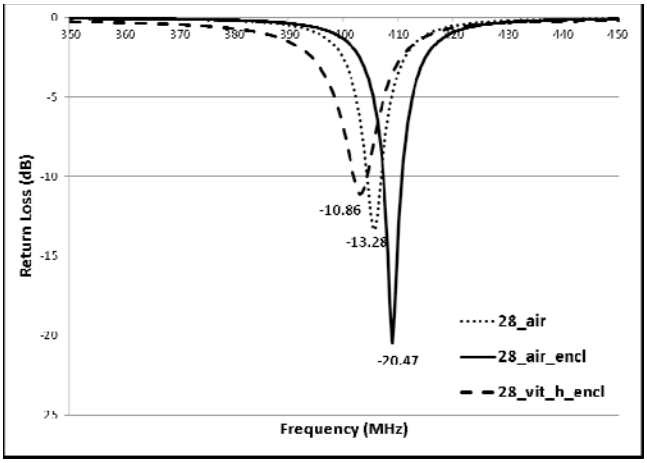

Figure. 2. The return loss of the antenna in three different simulation set ups.

TABLE I. MAXIMUM GAIN OF THE ANTENNA (SIMULATION)

Antenna	Max Gain (dB)
Air	-38.59
Air_encl	-38.15
Vit_h_encl	-40.33

III. ANTENNA FABRICATION AND MEASUREMENT

A. Fabrication

The antenna was fabricated by etching each RO3210 substrate separately. The first three layers were joined together by the two pins. One of the pins was an extension of the SMA connector pin, which acted as the feed pin. The top layer was attached using a combination of thinly spread adhesive material and a 24-hour pressure on the antenna to avoid any air gap in between the layers.

B. Measurement Procedure

The antenna was designed to work particularly at the surrounding material of Vitreous Humor fluid. Therefore, at the free space, the resonance frequency of the antenna will be outside the range (402 to 405 MHz). However, it is still a good indicator to see if the antenna is acting as predicted. At this stage, the antenna was not yet encapsulated by the PDMS layer and all the measurements were taken in free space.

The return loss measurement was conducted with the aid of Agilent E5071B network analyzer. A semi-rigid coaxial cable was connected to one of the ports at one end with the antenna at the other end.

For the radiation pattern measurement, a 6m x 3m anechoic chamber was utilized. A set of DM_105A_T3 dipole antennas was used as the source and the reference antenna. The distance separating the two antennas was approximately 4m, way beyond the far field boundary of each antenna. The receiving antenna, which in this case was

the antenna under test (AUT), was sitting on a rotator. The radiation patterns of the antenna, horizontally and vertically, were captured using Wiltron 37269A spectrum analyzer following a 360° rotation. Both E-field and H-field pattern were investigated by modification to the angle of the source antenna.

The actual gain of the antenna was calculated based on the maximum gain value obtained during the radiation pattern measurement in relative to the reference antenna gain. Mathematically, it was expressed as:

Gain (dBi) = Reference Gain + (Measured Level – Reference Level). (1)

The reference gain was in this case the half-wave dipole gain (2.15 dBi) while the measured level was the dipole gain during the calibration process (-23.63 dB).

C. Measurement Results

The measured return loss of the antenna at the free space was -18.44 dB at 433.33 MHz (Fig. 3). This result was shifted by 5.7% compared to the simulation result.

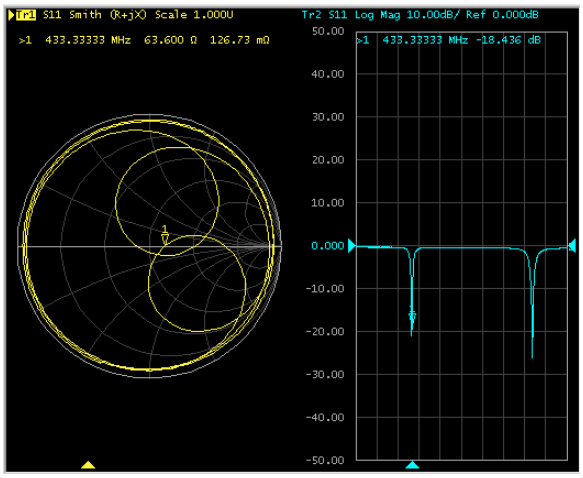

Figure. 3. Return loss of the antenna from the measurement.

The radiation pattern of the antenna in vertical orientation can be seen on Fig. 4 for both using the E-field source (Fig. 4a) and H-field source (Fig. 4b). It means, the top layer of the antenna was facing the source antenna in a clear line of sight. In vertical orientation, where the sides of the antenna were in line with the source direction, the patterns can be observed in Fig. 5.

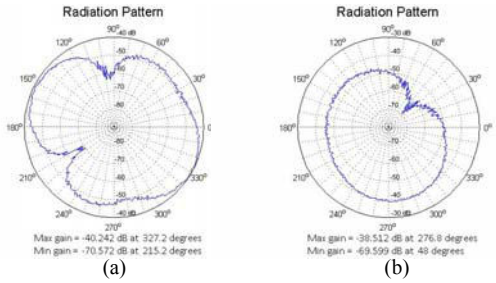

Figure. 4. Radiation pattern of the antenna with (a) E-field source and (b) H-field source in vertical orientation.

Equation (1) was implemented in the calculation process of the antenna gain, resulting maximum gain of -14.46 dBi, -16.4 dBi, -8.24 dBi, and -6.39 dBi for the radiation pattern observed in Fig. 4a, 4b, 5a, and 5b, respectively.

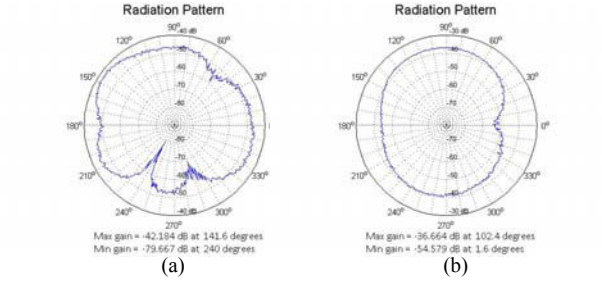

Figure. 5. Radiation pattern of the antenna with (a) E-field source and (b) H-field source in horizontal orientation.

IV. Analysis

As mentioned previously, the measured return loss of the antenna was slightly higher than the simulated one. The return loss of -18.44 dB occurred at 433.33 MHz frequency, 5.7% higher than expected. Even though the shift means that the antenna is outside the intended MICS band, it was still an encouraging result that can be beneficial for any future development. There were several aspects that may contribute to the discrepancy on the return loss, such as the use of different connector type between the simulation and the real antenna, imperfections in the fabrication process, and the presence of very thin adhesive material at the real antenna. The SMA connector used on the real antenna was built with two extended metal arms. One of the arms exceeded the substrate board (Fig. 6). In the simulation, these two arms did not exist and that may contribute to the slight shift of the resonance frequency. The antenna was hand-crafted by one of our lab technicians, with limited tools available. Hence it is impossible to maintain 100% accuracy in the fabrication process in regards to the alignment as well as other mechanical issues. The presence of adhesive substance to unite each layer together, however thin, was not simulated in the HFSS design. A shift in the return loss was possibly resulted due to this additional material.

In regards to the radiation pattern, the measured results resembled the omnidirectional pattern (E-field source) as expected from the simulation results, albeit there was clearly an issue with the alignment. For the H-field source, the pattern was expected to be a perfect circle that has the same gain for all the angles. However, the results showed a couple of dips in the pattern in addition to the uneven circular shape (Fig. 4b and 5b). There was also a discrepancy on the calculated gain values and the simulated results. The gain of the antenna was expected to be -38.59 dB (Table 1), but after the calculation using (1), the values were in the region of -14 to -16 dBi and -6 to -8 dBi for two different orientations.

Figure. 6. The SMA connector of the antenna

The huge gap on the antenna gain prompted questions on possible causes to that. The first reason may be that the anechoic chamber in where the measurements were taken is not compatible with this low frequency. There is no problem with the length of the room, which was clearly adequate considering the far field boundary. However, there may be a problem with the size of the sponge pyramids attached to the chamber walls. For lower frequency, bigger sponges are needed due to longer wavelengths. As a consequence of this arrangement, there were a lot of reflections from all over the room received by the AUT. Ultimately, it resulted in inaccurate gain reading from the antenna. Another factor that might contribute to the discrepancy was again the placement of the SMA connector at the back of the antenna. The presence of this connector might have some effect on the signal coming in to the antenna and therefore be responsible on some of the unwanted dips on the radiation patterns.

V. Future Works

This work is still at the beginning stage and it has shown some promising results from the measurements. The future works for this project includes setting up a free space measurement in a more suitable environment. The next step will be the encapsulation of the antenna, followed by the same set of measurements. Finally, a measurement in Vitreous Humor mimicking fluid will be conducted.

References

[1] A. H. A. Foundation. (2012, 14 March 2012). Facts on Macular Degeneration. Available: http://www.ahaf.org/macular/about/understanding/facts.html

[2] D. T. Hartong, E. L. Berson, and T. P. Dryja, "Retinitis pigmentosa," *Lancet,* vol. 368, pp. 1795-1809, 2006.

[3] V. Singh, A. Roy, R. Castro, K. McClure, R. Dai, R. Agrawal, R. J. Greenberg, J. D. Weiland, M. S. Humayun, and G. Lazzi, "On the thermal elevation of a 60-electrode epiretinal prosthesis for the blind," *IEEE Transactions on Biomedical Circuits and Systems,* vol. 2, pp. 289-300, 2008.

[4] V. Singh, A. Qusba, A. Roy, R. A. Castro, K. McClure, R. Dai, R. J. Greenberg, J. D. Weiland, M. S. Humayun, and G. Lazzi, "Specific absorption rate and current densities in the human eye and head induced by the telemetry link of an epiretinal prosthesis," *IEEE Transactions on Antennas and Propagation,* vol. 57, pp. 3110-3118, 2009.

[5] A. Caspi, J. D. Dorn, K. H. McClure, M. S. Humayun, R. J. Greenberg, and M. J. McMahon, "Feasibility study of a retinal prosthesis:Spatial vision with a 16-electrode implant," *Archives of Ophthalmology,* vol. 127, pp. 398-401, 2009.

[6] K. Sasagawa, M. Mitani, T. Sugiyama, T. Noda, T. Tokuda, and J. Ohta, "Implantable image sensor with light guide array plate for bioimaging," *Japanese Journal of Applied Physics,* vol. 49, 2010.

[7] Y. Terasawa, A. Uehara, E. Yonezawa, T. Saitoh, K. Shodo, M. Ozawa, Y. Tano, and J. Ohta, "A visual prosthesis with 100 electrodes featuring wireless signals and wireless power transmission," *IEICE Electronics Express,* vol. 5, pp. 574-580, 2008.

[8] D. C. Ng, T. Tokuda, S. Shiosaka, Y. Tano, and J. Ohta, "Implantable microimagers," *Sensors,* vol. 8, pp. 3183-3204, 2008.

[9] D. Tsai, J. W. Morley, G. J. Suaning, and N. H. Lovell, "Frequency-dependent reduction of voltage-gated sodium current modulates retinal ganglion cell response rate to electrical stimulation," *Journal of Neural Engineering,* vol. 8, 2011.

[10] S. A. Joarder, M. Abramian, G. J. Suaning, N. H. Lovell, and S. Dokos, "A continuum model of retinal electrical stimulation," *Journal of Neural Engineering,* vol. 8, 2011.

[11] H. Permana, Q. Fang, and I. Cosic, "3-layer implantable microstrip antenna optimised for retinal prosthesis system in MICS band," 2011, pp. 65-68.

[12] S. Gabriel, R. W. Lau, and C. Gabriel, "The dielectric properties of biological tissues: II. Measurements in the frequency range 10 Hz to 20 GHz," *Physics in Medicine and Biology,* vol. 41, pp. 2251-2269, 1996.